Journal of
Materials Chemistry C

Materials for optical, magnetic and electronic devices

Accepted Manuscript

This article can be cited before page numbers have been issued, to do this please use: D. Fang, T. Niu, Z. Chen, J. X. Zhang, Z. Zhang, S. Zhou, H. Liu, G. Chen, N. Fu, Q. Xue and J. Tao, *J. Mater. Chem. C*, 2025, DOI: 10.1039/D5TC02544C.

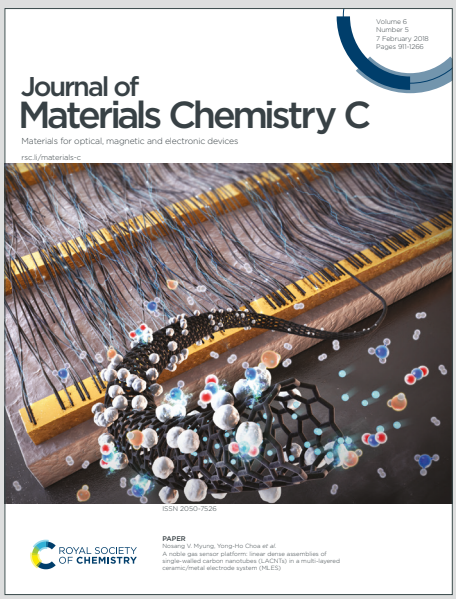

ROYAL SOCIETY OF CHEMISTRY

rsc.li/materials-c

View Article Online
DOI: 10.1039/D5TC02544C

Lignin Carbon Dot/Nanocellulose Films for Enhanced UV Stability and Efficiency in Perovskite Solar Cells through Selective Light Transmission, Blocking, and Conversion

Dongjun Fang[1†], Tianqi Niu[1†], Ziming Chen[1], Junxian Zhang[1], Ze Zhang[1], Shuang Zhou[1], Hao Liu[1, 2], Gang Chen[1], Nianqing Fu[1], Qifan Xue [1*], and Jinsong Tao[1, 2*]

[1] State Key Laboratory of Pulp and Paper Engineering and State Key Laboratory of Luminescent Materials and Devices, South China University of Technology, Guangzhou 510640, China. Email: qfxue@scut.edu.cn; jstao@scut.edu.cn

[2] Bengbu-SCUT Research Center for Advanced Manufacturing of Biomaterials, Bengbu, Anhui 233010, China.

[†] Equally contributed

KEYWORDS：Lignin carbon dot, nanocellulose, UV stability, efficiency, perovskite solar cells

View Article Online
DOI: 10.1039/D5TC02544C

Abstract

Perovskite solar cells (PSCs) are promising candidates for solar energy harvesting, but their poor UV stability poses a significant challenge. In this work, we developed lignin carbon dots (L-CD) embedded in nanocellulose (CNF) films to improve both the UV stability and efficiency of PSCs. The nanoscale CNF fibers provide high transparency to the films, allowing the transmission of visible (VIS) and most infrared (IR) light. Meanwhile, the aromatic structure of L-CD enables effective light absorption, blocking harmful UV and a portion of IR light. This combination ensures sufficient solar radiation while suppressing UV-induced degradation, increasing the retained efficiency of PSCs from 35% to 58%. Notably, the blocked UV and IR light were converted into VIS light, further boosting device performance. Key parameters, including short-circuit current density (Jsc), fill factor (FF), external quantum efficiency (EQE), and power conversion efficiency (PCE), were significantly enhanced. With the unique effects of optimal light transmission, blocking, and conversion, the L-CD/CNF films effectively mitigate UV exposure and broaden the range of solar light utilization, offering a green, cost-effective, and efficient strategy for fabricating high-performance PSCs.

View Article Online
DOI: 10.1039/D5TC02544C

1. Introduction

Perovskite solar cells (PSCs) have attracted significant attention for their exceptional light-harvesting capabilities, especially in the visible spectrum.[1] But PSCs are inherently unstable and prone to degradation under ultraviolet (UV) light, mainly due to the photocatalytic properties of the metal oxide-based electron transport layers. [2] Prolonged UV exposure can significantly reduce PSC performance, with studies reporting a 65% decrease in power conversion efficiency (PCE) after 1,000 hours of continuous UV irradiation.[3,4] This poor UV stability is a major barrier to PSC commercialization, making the improvement of UV stability crucial for their further development and practical application.

Significant efforts have been made to improve the UV stability of PSCs, and they generally fall into three categories: encapsulation of cells, UV filter layers, and down-conversion materials. (1) Encapsulation: Traditional encapsulation using polymers such as polyethylene terephthalate (PET) [5], polydimethylsiloxane (PDMS) [6], and ethylene vinyl acetate (EVA) [7] has been applied to improve UV stability, but these methods are not fully effective in blocking UV radiation.[8] (2) UV Filter Layers: Another approach involves adding UV filter layers, such as coating photocurable fluoropolymers on photoanode,[9] or adding cerium ions (Ce) in photoanode glass.[10] While effective at blocking UV light, these methods often reduce light transmittance, decreasing photocurrent. Additionally, rare earth elements like Ce are expensive and complex to process. Moreover, both encapsulation and UV filter layers only block UV light without reusing it. (3) Energy Conversion Materials: Down-conversion materials offer a more promising solution by converting UV light into visible light, which can be harvested by the PSCs, thereby enhancing photocurrents. Common materials include cadmium sulfide (CdS), cesium bromide (CsBr) [1], and carbon dots derived from organic sources like citric acid[11,12], glucose[13,14], dextrose[15], corn flour[16], and soybeans[17]. While

View Article Online
DOI: 10.1039/D5TC02544C

these materials containing heavy metals are expensive and harmful to the environment, and organic carbon dots often have weak UV absorption and fluorescence, limiting their effectiveness. In summary, each strategy above has merits, but none fully addresses the challenge of improving UV stability in PSCs. Encapsulation is incomplete, filter materials block UV without reusing them, and energy conversion materials can be costly, toxic, or lack sufficient efficiency. Therefore, the development of a green, cost-effective, and efficient solution for blocking UV light and improving UV stability of PSCs remains a challenge.

Lignin and its carbon dot derivatives and nanocellulose may offer a promising solution to the UV stability challenges in PSCs. Lignin, a major component of wood, is typically treated as waste in the papermaking industry and burned for energy. As the second most abundant natural aromatic polymer, lignin is rich in carbon and has a unique aromatic structure, making it an ideal precursor for carbon dot synthesis through hydrothermal methods. [18,19,20] Lignin-derived carbon dots (L-CDs) have several advantages: (i) they are nanoscale particles composed of sp^2/sp^3 carbon cores with diverse surface functional groups, providing excellent optical properties; (ii) they are low-cost, non-toxic, and environmentally friendly; (iii) their fabrication process is simple, green, and sustainable; (iv) they disperse uniformly in water; (v) they can absorb high-energy UV light and re-emit it as visible light; and (vi) their UV absorption properties can be tuned by modifying their structure and surface functional groups through oxidation, doping, or reduction. [21,22] On the other hand, cellulose nanofibers (CNFs), also derived from wood, provide further benefits. CNF surface is rich in hydroxyl and carboxyl groups, [20] which allow them to form a network-like structure to support other nanomaterials. CNFs are nanoscale and are easily dispersed in water, and can form highly transparent and mechanically strong films. [23,24,25] Given these properties, CNFs could be an

View Article Online
DOI: 10.1039/D5TC02544C

ideal substrate for L-CDs to create a transparent L-CD/CNF film to block UV light and enhance the UV stability of PSCs.

In this study, lignin was used as a raw material to synthesize lignin carbon dots (L-CDs) and develop L-CD/CNF films to block UV light to improve both the UV stability and efficiency of PSCs. The L-CDs were synthesized via hydrothermal methods, followed by doping and reduction treatments. The L-CDs were then incorporated into CNFs to create a transparent L-CD/CNF hybrid film. The film exhibits selective light transmission, blocking, and conversion properties, allowing visible (VIS) and most infrared (IR) light to pass through while blocking UV and partial IR radiation. The blocked UV and IR light is converted into visible light, which not only improves UV stability but also further boosts efficiency. This work offers a promising strategy for fabricating stable and efficient PSC devices.

View Article Online
DOI: 10.1039/D5TC02544C

Results and Discussion

2.1 Preparation and Application of Lignin Carbon Dot (L-CD) in PSCs

The preparation of lignin carbon dots (L-CD), cellulose nanofiber (CNF), and L-CD/CNF films and their application on PSCs are presented in **Figure 1**. Natural wood (Figure 1a) was used as the starting material to produce regular pulp fibers (Figure 1b) through pulp cooking processes. With the obtained pulp fibers, CNF (Figure 1c) can be separated through chemical and physical treatments. During pulp cooking processes, lignin with a natural aromatic structure and high carbon content (Figure 1d) can be obtained simultaneously. Through a hydrothermal method followed by pre-oxidation with H_2O_2, doping with $NH_3 \cdot H_2O$, or reduction with $NaHB_4$ (**Table 1**), lignin can be carbonized into different kinds of L-CD (Figure 1e) with abundant surface functional groups. [26,27,28] The prepared L-CD has excellent compatibility with CNF, and it can be embedded in CNF and form a uniform and transparent L-CD/CNF film (Figure 1f) that has outstanding mechanical properties and selective light transmission, blocking, and conversion performance. The L-CD/CNF films can also be formed on the ITO glass of the PSC photoanode by spray-coating processes. When the photoanode was coated with L-CD/CNF films, visible (VIS) and most infrared (IR) light can pass through, and UV and partial IR light (Near IR, NIR) was absorbed and blocked, and the UV light-induced degradation of PSCs was alleviated. And the UV stability of the device was improved. Meanwhile, the absorbed UV and NIR light were converted into visible light due to the energy conversion properties L-CD. As a result, the efficiency of PSCs was enhanced, too. The improvement of UV stability and efficiency is attributed to the low-cost, green, and effective L-CD/CNF films with unique optical effects.

Table 1 Preparation of L-CD through different treatments

	Treatments

View Article Online
DOI: 10.1039/D5TC02544C

Symbols	H_2O_2	$NH_3 \cdot H_2O$	$NaBH_4$
L-CD_0	No	No	No
L-CD_N	Yes	Yes	No
L-CD_R	Yes	Yes	Yes

2.2 Characterization of Lignin Carbon Dots and CNF

The structure and morphology of L-CD and CNF have a crucial influence on UV blocking and converting performance. **Figure 2**a presents the SEM image of reduced and N-doped L-CD (L-CD_R), showing L-CD_R has a nanoscale size of about 20 nm. Figures 2b and c illustrate the AFM images of L-CD_R, demonstrating that the prepared L-CD_R has a relatively uniform size and excellent dispersibility. And no obvious aggregation can be observed. Figure 2d plots the detailed size distribution of L-CD_R, demonstrating that the prepared L-CD_R mostly falls in the diameter range of 15-25 nm. Figure 2e presents the XRD pattern of L-CD_R. A broad low-intensity diffraction peak at $2\theta=23.1^\circ$ can be observed that corresponds to the (002) crystal plane of carbon (JCPDS card number 41-1487, main peak 23.1 °), indicating the prepared L-CD_R has an amorphous carbon structure. The interlayer spacing can be calculated with the Bragg equation, and it is 0.386 nm, which is larger than that of natural graphite (0.335 nm). This data is consistent with the previously reported results,[29] implying carbon dots have been prepared successfully, and they are amorphous carbon similar to graphene. Figures 2f and g present the AFM and SEM images of CNF, showing that the prepared CNF has a uniform morphology with a diameter of about 20 nm and a length of about 200 nm. The nanosized L-CD and CNF are beneficial to obtain high optical transparency hybrid films without loss of incident light.

2.3 Surface State Characterization of Lignin Carbon Dots

View Article Online
DOI: 10.1039/D5TC02544C

The UV absorption ability and fluorescence performance of L-CD are dependent on its structure and surface state. The infrared spectra of the synthesized lignin carbon dots of L-CD_R are presented in **Figure 3**a. The strong peak at 3423 cm^{-1} is ascribed to hydroxyl groups (O-H) stretching vibrations,[30] indicating there are abundant hydroxyl groups (O-H) on the surface of L-$CD_{R,}$ which is beneficial for the improvement of UV absorption and fluorescence performance.[22]The peak at 3236 cm^{-1} corresponds to N-H stretching vibrations. The peak at 1620 cm^{-1} corresponds to the C=O stretching vibration. The peaks at 1041, 1120, and 1170 cm^{-1} correspond to the vibrations of aromatic rings.[31] The absorption peaks in the range of 600~900 cm^{-1} correspond to C-H and C-O substituents on benzene rings. The results of infrared spectra show that the prepared L-CD_R has a similar structure and surface state to the original lignin. But the strong absorption peak of the hydroxyl group(O-H) should be ascribed to the reduction of $NaBH_4$.

The elements contained in carbon dots are also important for their UV absorption and fluorescence emission performance. To determine the elements in the carbon dots, we performed X-ray photoelectron spectroscopy (XPS) tests for L-CD_R (Figure 3b). C1s, O1s, and N1s peaks can be observed, indicating that the prepared L-CD_R contains C, O, and N, which also indicates N elements have been doped into carbon dots. Figures 3c-f present the C 1s, O 1s, N 1s and S 2p XPS spectra of L-CD_R. The peaks that appear at 284.8, 285.4 and 288.2 eV in Figure 3c of C 1s spectra correspond to C=C, C-N, and C=O groups. The peaks that appear at 532.1, 532.9 and 536.8 eV in Figure 3d of O1s spectra correspond to C=O, C-O and S=O groups. The appearance of C-O and C=O shows the carbon dots contain oxygen-containing polar groups such as hydroxyl (OH), carbonyl (C=O), carboxyl (COOH) and so on. The peak that appears at 400.4 eV in Figure 3e of N1s spectra corresponds to the N-H group, implying N has been doped in carbon dots successfully. The peaks appearing at 169.3eV(C-SO_2), 170.1eV(C-SO_3), 171.8eV(SO_4), 168.4eV(S=O) indicate

View Article Online
DOI: 10.1039/D5TC02544C

that S element is mainly introduced into carbon dots in the form of sulfonate (Figure 3f). The results of the XPS test are consistent with those of the infrared spectra tests. These results show the prepared carbon dots of L-CDR contain a large number of C=C groups and oxygen-containing groups such as hydroxyl groups (O-H). The results also show N was doped into carbon dots successfully. These surface groups and elements are crucial for the UV absorption and fluorescence emission of carbon dots.

2.4 UV Absorption, Conversion, and Fluorescence Performance of L-CDs

The absorption of visible light is crucial for the improvement of PSC performance. The more visible light absorbed, the higher efficiency of the PSC device will be. Because of their unique structure, carbon dots have the properties of converting the light beyond the visible light band into visible light, which can extend the unitization range of sunlight. Therefore, we characterized the photoluminescence, and up- and down-conversion properties of the prepared lignin carbon dots.

Figure 4a shows the fluorescence emission spectra of L-CD_0, L-CD_N, and L-CD_R with the same concentration under the excitation wavelength of 360 nm. It can be observed that the fluorescence intensity of L-CD_0 without H_2O_2 and $NH_3 \cdot H_2O$ treatments is weak, while the fluorescence intensity of L-CD_N and L-CD_R is significantly increased due to the doping of N, which should be attributed to the formation of more polycyclic aromatic hydrocarbon structures with pyridine as a unit that contains N elements. [21,32] In addition, the fluorescence intensity of L-CD_R was higher than that of L-CD_N, which should be attributed to the addition of $NaBH_4$ that reduces some of the carbonyl groups (-COOH) to hydroxyl groups (-OH). The increase of hydroxyl groups on the surface of carbon dots can increase the recombination efficiency of carriers, thereby increasing the fluorescence intensity.[33] Meanwhile, the doping of N elements of L-CD_N and L-CD_R causes the fluorescence spectra to red shift compared with that of L-CD_0, which should be

View Article Online
DOI: 10.1039/D5TC02544C

ascribed to the size effect of carbon dots. The introduction of N elements leads to a slight increase in the size of carbon dots,[34] while the fluorescence emission wavelength of carbon dots will undergo a red shift with the increase in size. [35] However, the fluorescence emission spectrum of L-CD_R undergoes a blue shift compared with L-CD_N, which should be attributed to the surface state change because of the reduction by $NaBH_4$.[36]

In order to explore the fluorescent properties of L-CD_R, we further performed 3D fluorescence spectroscopy tests (Figures 4b and c). It can be seen that the L-CD_R demonstrates excitation wavelength-dependent down-conversion properties. When the L-CD_R is excited by the light in the UV band with a wavelength from 300 to 400 nm, the fluorescence emission is concentrated in the visible light range with a wavelength from 400 to 600 nm, showing the L-CD_R has outstanding energy down-conversion properties. With the increase of excitation wavelength, the fluorescence emission peak gradually red-shifts, and the fluorescence intensity increases first and then decreases. The fluorescence intensity reaches the maximum value of 111000 at the emission wavelength of 452 nm under the excitation wavelength of 350 nm. The results indicate the L-CD_R has outstanding energy down-conversion and fluorescence emission properties in the range of UV band, which should be related to the electron transition at different energy levels in UV band. [37]

Meanwhile, we also performed fluorescence spectrum tests for up-conversion properties. Figure 4d presents the fluorescence emission spectra of L-CD_0, L-CD_N, and L-CD_R with the same concentration under the excitation wavelength of 800 nm. It can be seen that the fluorescence intensity of L-CD_R and L-CD_N is much higher than that of L-CD_0, which is attributed to the doping of N and S elements. The sharp peak near 400 nm in the PL spectra of L-CD_0, L-CD_N, and L-CD_R should originate from excitation light leakage or Rayleigh scattering. The 3D fluorescence spectra

View Article Online
DOI: 10.1039/D5TC02544C

of L-CD_R that were excited by near-infrared (NIR) wavelength ranging from 700 to 900 nm are shown in Figures 4e and f. Tiny fluorescence emission peaks in the visible light range of 400-600 nm can be observed, and the peaks gradually blue-shift with the increase of the excitation wavelength. And the maximum fluorescence intensity excited by NIR wavelength is about 2000, which is far lower than 111000 obtained by the UV light excitation. The results indicate the prepared L-CD_R has weak energy up-conversion ability, which is likely ascribed to the contribution of the stray light caused by second-order diffraction of the monochromator.

The fluorescence quantum yield of L-CD_0, L-CD_N, and L-CD_R is shown in Figure 4g. L-CD_R treated with H_2O_2, $NH_3 \cdot H_2O$ and $NaBH_4$ demonstrates the highest fluorescence quantum yield of 32.57%. L-CD_N treated with H_2O_2, and $NH_3 \cdot H_2O$ has a fluorescence quantum yield of 25.43%. L-CD_0 without any treatments has the lowest fluorescence quantum yield of 5.44%. Figures 4h and i present the digital photo images of the aqueous solution of L-CD_0, L-CD_N, and L-CD_R with the same concentration under daylight and UV light excitation. It can be found that L-CD_R emits the strongest fluorescence than L-CD_N and L-CD_0. The image results are consistent with the results of their quantum yield.

2.5 UV Absorptivity of L-CD Aqueous Dispersion and L-CD/CNF Films

The UV absorptivity of lignin carbon dots is crucial for the UV stability of PSCs. We tested the UV absorption performance of various L-CD aqueous dispersion for proper L-CD/CNF film fabrication. **Figure 5**a presents the ultraviolet-visible absorption spectra of L-CD_0, L-CD_N, and L-CD_R dispersion. Three kinds of carbon dots have obvious absorption in UV band. And L-CD_R shows the strongest absorption performance, followed by L-CD_N and L-CD_0. Usually, strong UV absorption will lead to strong fluorescence emission.[38] Strong UV absorption is beneficial for the improvement of PSC's stability, and strong fluorescence emission is good for the enhancement of

View Article Online
DOI: 10.1039/D5TC02544C

PSC's efficiency. Three kinds of carbon dots have an absorption peak at 285 nm, which could correspond to the π→π* electron transition of the aromatic structure of the benzene rings of lignin. In addition, L-CD_R and L-CD_N have a strong absorption peak at 224 nm, which should be ascribed to the *n*→π* electron transition of the *p*-π conjugated structure of lignin carbon dots. The existence of *p*-π conjugated structure implies the existence of unsaturated aliphatic structures such as C=C-OH and C=C-OR in L-CD_N and L-CD_R.

We further investigated the effect of some parameters on the UV absorption ability of carbon dots such as concentration, pH value, and the amount of H_2O_2. Figure 5b presents the effect of L-CD_R concentration on its UV absorptivity. When the concentration is below 100mg/L, the UV absorptivity of L-CD_R dispersion increases with the increase of its concentration. Figure 5c presents the effect of pH value on UV absorptivity. When the pH increases from 0 to 14, the UV absorptivity of the L-CD_R dispersion remains stable, showing that the pH of the L-CD_R dispersion has no obvious impact on the UV absorptivity. In the preparation of L-CD_R, we pre-treated lignin with H_2O_2, which not only oxidized the surface functional group of lignin, but also helped to cut the large molecules into small fragments. Figure 5d presents the effect of the amount of H_2O_2 on the UV absorptivity of L-CD_R. When the amount of H_2O_2 increases from 2 to 6 ml, the UV absorptivity of L-CD_R decreases gradually. When the amount of H_2O_2 exceeds 6 ml, the UV absorptivity of L-CD_R decreases greatly. Too much H_2O_2 likely has an adverse effect on conjugated structures, which determine the UV absorptivity of L-CD_R. [32] Therefore, it is necessary to strictly control the dosage of H_2O_2 to prevent conjugated structures from being destroyed. [41]

The lignin carbon dots are finally blended with CNF and coated on the ITO glass to form L-CD/CNF hybrid films; thus, the performance of the films was also investigated. Figure 5e is the UV absorption spectra of the hybrid films of L-CD_0, L-CD_N, and L-CD_R with CNF. It can be seen

View Article Online
DOI: 10.1039/D5TC02544C

that L-CD_R/CNF films have the strongest UV absorption. Figure 5f presents the UV absorption spectra of the L-CD_R/CNF hybrid films with different volumes of L-CD_R. With the increase in the volume amount of L-CD_R in the hybrid films, the UV absorptivity increases gradually. Figure 5g shows the effects of the amount of H_2O_2 during the preparation of carbon dots on the UV absorptivity of the final L-CD_R/CNF films. The UV absorptivity of the L-CD_R/CNF films decreases with the increase in the amount of H_2O_2. The results are roughly consistent with those shown in Figure 5d.

The effects of the hybrid films coated on ITO glass on the optical transmittance were also investigated (Figure 5h). The transmittance of the ITO glass with and without L-CD_R/CNF films was measured. The results show that the ITO glass coated with L-CD_R/CNF films demonstrates a close transmittance to that of bare ITO glass. Their transmittance is all higher than 85% during visible light wavelength of 400~800 nm, showing L-CD_R/CNF films have a high optical transmittance. And L-CD_R/CNF coating has almost not caused the incident light loss for ITO glass. The high transmittance of L-CD_R/CNF should be ascribed to the nanometer size of L-CD_R, the high transparency of CNF, and the outstanding dispersion of L-CD_R in CNF. The inset picture in Figure 5h is the digital photo image of ITO glass coated with and without L-CD_R/CNF films. They all show outstanding transparency with no obvious difference. The fluorescence quantum efficiency of the L-CD_R/CNF film was measured and it is 10%, which is lower than that of the L-CD_R/CNF solution (32.57%) due to matrix interference or reabsorption effects. Meanwhile, the L-CD_R/CNF film demonstrates relatively stable photostability under continuous illumination from a solar simulator. Based on the results, L-CD_R/CNF films can be covered on the photoanode glass to conduct further device tests.

2.6 Effects of the L-CDR/CNF Films on PSC Device Performance

View Article Online
DOI: 10.1039/D5TC02544C

To investigate the effects of L-CD films on the PSC performance, we fabricated PSC devices based on the ITO glass coated with L-CD_R/CNF with the device structure ITO/ SnO_2/perovskite/spiro-OMeTAD/MoO_3/Ag (**Figure 6**a). The inset picture is a digital photo image of the top and back sides of the device. Meanwhile, we fabricated the devices without L-CD_R/CNF as control samples to conduct a comparison analysis.

Figure 6b presents the J-V curves of the devices with and without L-CD_R/CNF films. The short-circuit photocurrent (J_{SC}) of the devices coated with L-CD_R/CNF is slightly improved compared with that of those without L-CD_R/CNF. The improved J_{SC} leads to a slight increase in fill factor (FF) and power conversion efficiency (PCE), with the FF increasing from 74.00 to 74.88, and the PCE increased from 18.25 to 18.60. The detailed photovoltaic parameters of the devices are listed in the inset table in Figure 6b. Figure 6c presents the external quantum efficiency (EQE) spectra of the devices with and without L-CD_R/CNF with their integrated current density (J_{SC}) plots. In the visible light band, the EQE and J_{SC} of the PSCs with L-CD_R/CNF are roughly all enhanced, which is attributed to the energy conversion properties of L-CD_R in the UV and NIR wavelength region. [39]

We investigated the effects of L-CD_R/CNF films on the stability of PSC devices under continuous irradiation of sunlight (AM 1.5G) in air (Figure 6d). The devices coated with L-CD_R/CNF films still retain more than 58% of the initial PCE after continuous irradiation for 300 hours, while the device without L-CD_R/CNF films (control sample) only maintained 35% of the initial PCE after exposure to the same conditions, which shows that the L-CD_R/CNF films can significantly improve the stability of PSC devices. The inset pictures in Figure 6d present the digital photo images of the devices before and after continuous irradiation. It can be seen that the device with L-CD_R/CNF films demonstrates no obvious degradation. However, the device without

View Article Online
DOI: 10.1039/D5TC02544C

L-CD_R/CNF (control sample) demonstrates obvious degradation. It should be attributed to the L-CD_R/CNF films that can block the UV light and impede UV-induced degradation. Therefore, the results show that the coated L-CD_R/CNF films can elongate the lifetime of PSCs, enabling PSCs to take a small step toward commercialization.

Finally, we have demonstrated that the L-CD_R/CNF films possess excellent UV light blocking and conversion properties, which can enhance the efficiency and stability of PSC devices. Compared to other CD-based composite films, L-CD_R/CNF films also stand out due to their green origin, mechanical robustness, optical clarity, and biodegradability, making them particularly suitable for sustainable optoelectronic and light-filtering applications. With these environmental and functional advantages, L-CD_R/CNF films are highly competitive for eco-friendly photovoltaic material fabrication.

View Article Online
DOI: 10.1039/D5TC02544C

4. Conclusions

In summary, we have developed an efficient method to block UV light and improve both the stability and efficiency of PSCs using lignin carbon dots/nanocellulose (L-CD/CNF) films. The high transparency of CNF films ensures optimal light transmission, while the excellent optical absorption properties of L-CDs selectively block harmful UV and partial IR radiation, significantly improving device stability from 35% to 58%. Additionally, the strong light conversion capabilities of L-CDs enable the conversion of blocked UV and IR light into visible light, further enhancing the PCE from 18.25% to 18.60% and broadening the usable solar spectrum. This green, cost-effective approach offers a promising pathway for fabricating PSCs with enhanced stability and efficiency, contributing to more sustainable solar energy harvesting.

View Article Online
DOI: 10.1039/D5TC02544C

4. Experimental section

4.1 Preparation of Lignin Carbon Dots: Lignin (1g) was dissolved in deionized water (40 mL). Hydrogen peroxide (6 mL) was added and kept stirring for 12 hours at 25°C in a dark room. Ammonia liquor (10 mL) was added and the mixed solution was transferred to a Teflon-lined stainless-steel autoclave. The autoclave was kept in an oven to conduct carbonization at 180°C for 12 h. Then the autoclave was cooled down to room temperature. The obtained solution was centrifuged at 12000 rpm for 20 min to remove large particles and the light brown supernatant was collected. The supernatant solution was filtered with a syringe filter with a 0.22 μm nylon membrane and the filtered solution was collected. $NaBH_4$(0.5 g) was added to the filtered solution and stirred at room temperature for 12 h to reduce the carbon dots. Then the solution was dialyzed for 24 h to remove excess $NaBH_4$. The obtained reduced solution was freeze-dried into powder. And the freeze-dried powder was stored in a refrigerator at 4 °C. And the L-CD was named L-CD_R. Meanwhile, L-CD_N was prepared in a similar way to L-CD_R fabrication processes, but not add $NaBH_4$ (0.5 g). And L-CD_0 was prepared too but not adding H_2O_2(6 mL), $NH_3 \cdot H_2O$ (10 mL) and $NaBH_4$ (0.5 g) (Table 1).

4.2 Preparation of L-CD/CNF Films: The free-dried carbon dot powder was dissolved in deionized water to prepare a dispersion with a certain concentration. Then the carbon dot dispersion was added to CNF dispersion (0.51 wt.%) with different proportions to prepare L-CD/CNF solution. The L-CD/CNF solution was placed in a high-frequency ultrasonic cell disruptor for 20 minutes to generate a homogeneous dispersion. The homogeneous dispersion was poured into a Petri dish, then transferred to an oven and kept there at 40 °C for 24 h to obtain a transparent hybrid film.

View Article Online
DOI: 10.1039/D5TC02544C

4.3 Manufacturing of PSCs*:* The traditional n-i-p type perovskite solar cells with a structure of ITO/SnO_2/ Perovskite/Spiro-OMeTAD/MoO_3/Ag) were fabricated. The ITO glass (1.5cm×1.5cm) was ultrasonically cleaned for 30 min with ethanol and ultrabare water, and then dried in an oven for 10~15 min at 70℃. The nanosized SnO_2 solution was spin-coated on the cleaned ITO glass substrate at 3000rpm for 30 s and then annealed for 20 min at 150℃ to prepare ETLs with a thickness of 30nm. The prepared perovskite precursor solution (1.5 M) was uniformly spin-coated on SnO_2 ETLs (the spin-coating processes were divided into two stages: first stage, 1000 RPM, 10 s; second stage, 4000 RPM, 40 s). Then the coated perovskite layers were annealed for 30 minutes at 110℃ to prepare the perovskite light absorption layers with a thickness of 700nm. After the layers were cooled down to room temperature, the Spiro-OMeTAD solution was spin-coated on the perovskite light absorption layers at 5000 rpm for 30 seconds to prepare hole transport layers with a thickness of 150 nm. MoO_3 (12nm) and Ag electrode (80nm) were deposited in an evaporation chamber with a thermal evaporation method. The active area of each device was 0.05 cm^2. A MoO_3 buffer layer (12nm) and an Ag electrode (80nm) were deposited on the hole transport layers in an evaporation chamber by thermal evaporation. And the PSC devices were obtained. The prepared L-CD_R/CNF dispersion was spin-coated on the photoanode ITO glass of the obtained PSC devices and annealed at 100°C, L-CD_R/CNF films were formed on the ITO glass of PSC devices. To quantify the effect of the L-CD_R/CNF films on the overall device performance, forty PSC devices with L-CD_R/CNF films were tested.

4.3 Photovoltaic performance testing of PSCs*:* The photovoltaic performance of the perovskite solar cells was tested by a solar simulator system. The short-circuit current density (J_{SC}), open-circuit voltage (V_{OC}), fill factor (FF), and power conversion efficiency (PCE) were measured under the simulated solar radiation intensity of 100 mW/cm^2. The scanning rate is 0.3V s^{-1}, the delay

View Article Online
DOI: 10.1039/D5TC02544C

time is 10-50ms, and the width of the scanning step is 0.02V. Before testing, the device was calibrated with a single-crystal silicon cell for light intensity. The EQE was measured by a quantum efficiency measuring instrument. The J-V curves of the devices in the dark state were measured by a KEITHLEY 2400 digital source meter.

4.4 Characterizations: The L-CD solution and L-CD/CNF films were characterized by SEM (Zeiss, EVO 18, Germany) and AFM (Bruker, Multimode, Germany). The crystal structure of L-CD was measured by a D8 advanced X-ray diffractometer (Bruker, Germany) with a testing range of 10-60°. The functional groups of L-CD were characterized by an infrared spectrometer (Bruker, Tensor27/Hyperion, Germany) with a testing range of 500-3800 cm^{-1} and under total reflection testing mode. The element composition and element valence of L-CD were measured by an X-ray photoelectron spectrometer with a testing range of 0-800eV. The fluorescence properties of the L-CD were measured by a fluorescence spectrometer (FluoroMax-4, Horiba, American). The absolute quantum yield (QY) of the films and L-CD solutions was measured under ambient conditions using a Hamamatsu C9920-02G integrating sphere system, coupled with a 150 W xenon lamp and a PMA-12 photonic multichannel analyzer. The UV absorption properties were measured by an Ultraviolet-visible infrared spectrophotometer (Lambda 950, PerkinElmer, American) in the range of 200-900 nm.

AUTHOR INFORMATION

Supporting Information. No.

Corresponding Author

*To whom correspondence should be addressed. E-mail: *jstao@scut.edu.cn* and *qfxue@scut.edu.cn*

Author Contributions

View Article Online
DOI: 10.1039/D5TC02544C

The manuscript was written with the contributions of all authors. J. T. provided the original idea and is responsible for the organization and supervision of this work.

Data availability

The authors confirm that the data supporting this study are available in figures, tables, and schemes within the article body and ESI.

Statement of contributions:

J. T. provided the original idea and is responsible for the organization and supervision of this work. J. T., Q.X, D.F., and T.N. designed experiments; D. F. and T. N. carried out experiments; Z.C., S.Z, Z.Z., and J.Z. assisted in the use of testing instruments; D. F. and T. N. analyzed experimental results and wrote the manuscript; H. L., G.C., N.F., Q.X., and J.T. reviewed and directed the paper writing; J.Z. was responsible for the typesetting and submission of the manuscript.

Conflict of Interest

The authors declare no interest conflict. They have no known competing financial interests or personal relationships that could have appeared to influence the work reported in this paper.

Acknowledgments

This work is funded by Guangdong Basic and Applied Basic Research Foundation (2023A1515011388). Q. Xue acknowledges the open research fund of Songshan Lake Materials Laboratory (2021SLABFN17), Guangdong Provincial Key Laboratory of New and Renewable Energy Research and Development (E239kf0901), Guangdong Basic and Applied Basic Research Foundation for Distinguished Young Scholar (2021B1515020028), National Natural Science Foundation of China (22379045) and TCL Young Scholars Program.

Received: ((will be filled in by the editorial staff))
Revised: ((will be filled in by the editorial staff))
Published online: ((will be filled in by the editorial staff))

View Article Online
DOI: 10.1039/D5TC02544C

References

(1) Li, W.; Zhang, W.; Van Reenen, S.; Sutton, R. J.; Fan, J.; Haghighirad, A. A.; Johnston, M. B.; Wang, L.; Snaith, H. J. Enhanced UV-Light Stability of Planar Heterojunction Perovskite Solar Cells with Caesium Bromide Interface Modification. *Energy Environ. Sci.* **2016**, *9* (2), 490–498.

(2) Dong, X.; Fang, X.; Lv, M.; Lin, B.; Zhang, S.; Wang, Y.; Yuan, N.; Ding, J. Method for Improving Illumination Instability of Organic–inorganic Halide Perovskite Solar Cells. *Sci. Bull.* **2016**, *61* (3), 236–244.

(3) Lee, S.-W.; Kim, S.; Bae, S.; Cho, K.; Chung, T.; Mundt, L. E.; Lee, S.; Park, S.; Park, H.; Schubert, M. C.; et al. UV Degradation and Recovery of Perovskite Solar Cells. *Sci. Rep.* **2016**, *6* (1), 38150.

(4) Mohamad Noh, M. F.; Teh, C. H.; Daik, R.; Lim, E. L.; Yap, C. C.; Ibrahim, M. A.; Ahmad Ludin, N.; Mohd Yusoff, A. R. Bin; Jang, J.; Mat Teridi, M. A. The Architecture of the Electron Transport Layer for a Perovskite Solar Cell. *Journal of Materials Chemistry C*. 2018, 682–712.

(5) Cheacharoen, R.; Boyd, C. C.; Burkhard, G. F.; Leijtens, T.; Raiford, J. A.; Bush, K. A.; Bent, S. F.; McGehee, M. D. Encapsulating Perovskite Solar Cells to Withstand Damp Heat and Thermal Cycling. *Sustain. Energy Fuels* **2018**, *2* (11), 2398–2406.

(6) Liu, Z.; Sun, B.; Shi, T.; Tang, Z.; Liao, G. Enhanced Photovoltaic Performance and Stability of Carbon Counter Electrode Based Perovskite Solar Cells Encapsulated by PDMS. *J. Mater. Chem. A* **2016**, *4* (27), 10700–10709.

(7) Cheacharoen, R.; Rolston, N.; Harwood, D.; Bush, K. A.; Dauskardt, R. H.; McGehee, M. D. Design and Understanding of Encapsulated Perovskite Solar Cells to Withstand Temperature Cycling. *Energy Environ. Sci.* **2018**, *11* (1), 144–150.

(8) Weerasinghe, H. C.; Dkhissi, Y.; Scully, A. D.; Caruso, R. A.; Cheng, Y. B. Encapsulation for Improving the Lifetime of Flexible Perovskite Solar Cells. *Nano Energy* **2015**, *18*, 118–125.

(9) Bella, F.; Griffini, G.; Correa-Baena, J. P.; Saracco, G.; Grätzel, M.; Hagfeldt, A.; Turri, S.; Gerbaldi, C. Improving Efficiency and Stability of Perovskite Solar Cells with Photocurable Fluoropolymers. *Science.* **2016**, *354* (6309), 203–206.

(10) Kempe, M. D.; Moricone, T.; Kilkenny, M. Effects of Cerium Removal from Glass on Photovoltaic Module Performance and Stability. In *Reliability of Photovoltaic Cells, Modules, Components, and Systems II*; 2009,7412, 74120Q.

View Article Online
DOI: 10.1039/D5TC02544C

(11) Wang, H.; Sun, P.; Cong, S.; Wu, J.; Gao, L.; Wang, Y.; Dai, X.; Yi, Q.; Zou, G. Nitrogen-Doped Carbon Dots for "green" Quantum Dot Solar Cells. *Nanoscale Res. Lett.* **2016**, *11* (1), 27.

(12) Riaz, R.; Ali, M.; Maiyalagan, T.; Anjum, A. S.; Lee, S.; Ko, M. J.; Jeong, S. H. Dye-Sensitized Solar Cell (DSSC) Coated with Energy down Shift Layer of Nitrogen-Doped Carbon Quantum Dots (N-CQDs) for Enhanced Current Density and Stability. *Appl. Surf. Sci.* **2019**, *483*, 425–431.

(13) Tang, Q.; Zhu, W.; He, B.; Yang, P. Rapid Conversion from Carbohydrates to Large-Scale Carbon Quantum Dots for All-Weather Solar Cells. *ACS Nano* **2017**, *11* (2), 1540–1547.

(14) Marinovic, A.; Kiat, L. S.; Dunn, S.; Titirici, M. M.; Briscoe, J. Carbon-Nanodot Solar Cells from Renewable Precursors. *ChemSusChem* **2017**, *10* (5), 1004–1013.

(15) Maxim, A. A.; Sadyk, S. N.; Aidarkhanov, D.; Surya, C.; Ng, A.; Hwang, Y.-H.; Atabaev, T. S.; Jumabekov, A. N. PMMA Thin Film with Embedded Carbon Quantum Dots for Post-Fabrication Improvement of Light Harvesting in Perovskite Solar Cells. *Nanomaterials* **2020**, *10* (2), 291.

(16) Teymourinia, H.; Salavati-Niasari, M.; Amiri, O.; Farangi, M. Facile Synthesis of Graphene Quantum Dots from Corn Powder and Their Application as down Conversion Effect in Quantum Dot-Dye-Sensitized Solar Cell. *J. Mol. Liq.* **2018**, *251*, 267–272.

(17) Meng, Y.; Zhang, Y.; Sun, W.; Wang, M.; He, B.; Chen, H.; Tang, Q. Biomass Converted Carbon Quantum Dots for All-Weather Solar Cells. *Electrochim. Acta* **2017**, *257*, 259–266.

(18) Carrier, M.; Loppinet-Serani, A.; Denux, D.; Lasnier, J. M.; Ham-Pichavant, F.; Cansell, F.; Aymonier, C. Thermogravimetric Analysis as a New Method to Determine the Lignocellulosic Composition of Biomass. *Biomass and Bioenergy* **2011**, *35* (1), 298–307.

(19) Tuck, C. O.; Pérez, E.; Horváth, I. T.; Sheldon, R. A.; Poliakoff, M. Valorization of Biomass: Deriving More Value from Waste. *Science*. 2012, 337(6095), 695–699.

(20) Jia, D.; Xie, J.; Dirican, M.; Fang, D.; Yan, C.; Liu, Y.; Li, C.; Cui, M.; Liu, H.; Chen, G.; et al. Highly Smooth , Robust , Degradable and Cost-Effective Modified Lignin-Nanocellulose Green Composite Substrates for Flexible and Green Electronics. *Compos. Part B Eng.* **2022**, *236*, 109803.

(21) Qian, Z.; Ma, J.; Shan, X.; Feng, H.; Shao, L.; Chen, J. Highly Luminescent N-Doped Carbon Quantum Dots as an Effective Multifunctional Fluorescence Sensing Platform. *Chem. - A Eur. J.* **2014**, *20* (8), 2254–2263.

(22) Tian, R.; Hu, S.; Wu, L.; Chang, Q.; Yang, J.; Liu, J. Tailoring Surface Groups of Carbon Quantum Dots to Improve Photoluminescence Behaviors. In *Applied Surface Science*; 2014, 301, 156–160.

View Article Online
DOI: 10.1039/D5TC02544C

(23) Yu, H.; Tian, Y.; Dirican, M.; Fang, D.; Yan, C.; Xie, J.; Jia, D.; Liu, Y.; Li, C.; Cui, M.; et al. Flexible, Transparent and Tough Silver Nanowire/nanocellulose Electrodes for Flexible Touch Screen Panels. *Carbohydr. Polym.* **2021**, *273*, 118539.

(24) Fang, D.; Yu, H.; Dirican, M.; Tian, Y.; Xie, J.; Jia, D.; Yan, C.; Liu, Y.; Li, C.; Liu, H.; et al. Disintegrable , Transparent and Mechanically Robust High-Performance Antimony Tin Oxide/nanocellulose/polyvinyl Alcohol Thermal Insulation Films. *Carbohydr. Polym.* **2021**, *266*, 118175.

(25) Yu, H.; Fang, D.; Dirican, M.; Wang, R.; Tian, Y.; Chen, L.; Liu, H.; Wang, J.; Tang, F.; Asiri, A. M.; et al. Binding Conductive Ink Initiatively and Strongly: Transparent and Thermally Stable Cellulose Nanopaper as a Promising Substrate for Flexible Electronics. *ACS Appl. Mater. Interfaces* **2019**, *11* (22), 20281–20290.

(26) Liu, H.; Ye, T.; Mao, C. Fluorescent Carbon Nanoparticles Derived from Candle Soot. *Angew. Chemie* **2007**, *119* (34), 6593–6595.

(27) Ray, S. C.; Saha, A.; Jana, N. R.; Sarkar, R. Fluorescent Carbon Nanoparticles: Synthesis, Characterization, and Bioimaging Application. *J. Phys. Chem. C* **2009**, *113* (43), 18546–18551.

(28) Wang, X.; Cao, L.; Yang, S. T.; Lu, F.; Meziani, M. J.; Tian, L.; Sun, K. W.; Bloodgood, M. A.; Sun, Y. P. Bandgap-like Strong Fluorescence in Functionalized Carbon Nanoparticles. *Angew. Chemie - Int. Ed.* **2010**, *49* (31), 5310–5314.

(29) Xu, L.; Cheng, C.; Yao, C.; Jin, X. Flexible Supercapacitor Electrode Based on Lignosulfonate-Derived Graphene Quantum Dots/graphene Hydrogel. *Org. Electron.* **2020**, *78*, 105407.

(30) Arcudi, F.; Dordevic, L.; Prato, M. Synthesis, Separation, and Characterization of Small and Highly Fluorescent Nitrogen-Doped Carbon Nanodots. *Angew. Chemie - Int. Ed.* **2016**, *55* (6), 2107–2112.

(31) Zhao, C.; Qiao, X.; Shao, Q.; Hassan, M.; Ma, Z.; Yao, L. Synergistic Effect of Hydrogen Peroxide and Ammonia on Lignin. *Ind. Crops Prod.* **2020**, *146*, 112177.

(32) Tang, J.; Zhang, J.; Zhang, Y.; Xiao, Y.; Shi, Y.; Chen, Y.; Ding, L.; Xu, W. Influence of Group Modification at the Edges of Carbon Quantum Dots on Fluorescent Emission. *Nanoscale Res. Lett.* **2019**, *14* (1), 241.

(33) Zheng, H.; Wang, Q.; Long, Y.; Zhang, H.; Huang, X.; Zhu, R. Enhancing the Luminescence of Carbon Dots with a Reduction Pathway. *Chem. Commun.* **2011**, *47* (38), 10650–10652.

View Article Online
DOI: 10.1039/D5TC02544C

(34) Liu, J.; Liu, X.; Luo, H.; Gao, Y. One-Step Preparation of Nitrogen-Doped and Surface-Passivated Carbon Quantum Dots with High Quantum Yield and Excellent Optical Properties. *RSC Adv.* **2014**, *4* (15), 7648–7654.

(35) Li, H.; He, X.; Kang, Z.; Huang, H.; Liu, Y.; Liu, J.; Lian, S.; Tsang, C. H. A.; Yang, X.; Lee, S. T. Water-Soluble Fluorescent Carbon Quantum Dots and Photocatalyst Design. *Angew. Chemie - Int. Ed.* **2010**, *49* (26), 4430–4434.

(36) Hu, S.; Trinchi, A.; Atkin, P.; Cole, I. Tunable Photoluminescence across the Entire Visible Spectrum from Carbon Dots Excited by White Light. *Angew. Chemie - Int. Ed.* **2015**, *54* (10), 2970–2974.

(37) Zhang, Y.; Yuan, R.; He, M.; Hu, G.; Jiang, J.; Xu, T.; Zhou, L.; Chen, W.; Xiang, W.; Liang, X. Multicolour Nitrogen-Doped Carbon Dots: Tunable Photoluminescence and Sandwich Fluorescent Glass-Based Light-Emitting Diodes. *Nanoscale* **2017**, *9* (45), 17849–17858.

(38) Hu, G.; Lei, B.; Jiao, X.; Wu, S.; Zhang, X.; Zhuang, J.; Liu, X.; Hu, C.; Liu, Y. Synthesis of Modified Carbon Dots with Performance of Ultraviolet Absorption Used in Sunscreen. *Opt. Express* **2019**, *27* (5), 7629.

(39) Nazim, M.; Kim, B.; Lee, S.; Min, B. K.; Kim, J. H. UV-Curable Polymer-QD Flexible Films as the Downconversion Layer for Improved Performance of Cu(In,Ga)Se2Solar Cells. *Energy and Fuels* **2020**, *34* (11), 14581–14590.

View Article Online
DOI: 10.1039/D5TC02544C

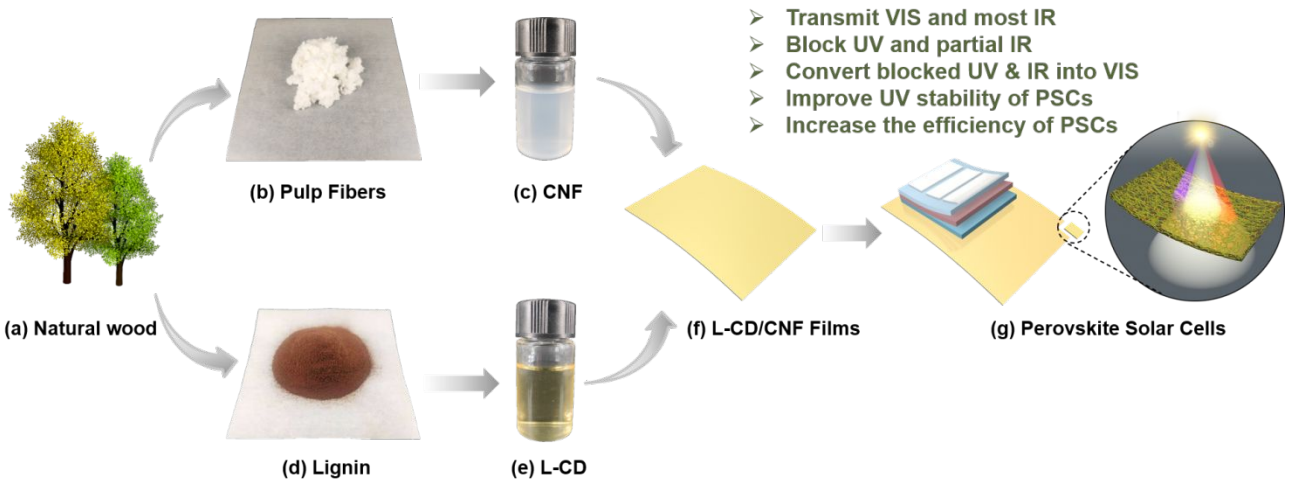

Figure 1. Preparation of lignin carbon dots(L-CD)/nanocellulose (CNF) films and their application on perovskite solar cells (PSCs). (**a**) Starting material of natural wood. (**b**) Pulp fibers. (**c**) Cellulose nanofiber (CNF) isolated from natural wood. (**d**) Lignin separated from natural wood. (**e**) L-CD aqueous solution with low cost, non-toxicity, and excellent dispersibility. (**f**) L-CD/CNF films. (**g**) PSCs with improved UV stability and efficiency. The improvement of stability and efficiency of PSCs is attributed to the L-CD/CNF films with selective light transmission, blocking, and conversion properties.

View Article Online
DOI: 10.1039/D5TC02544C

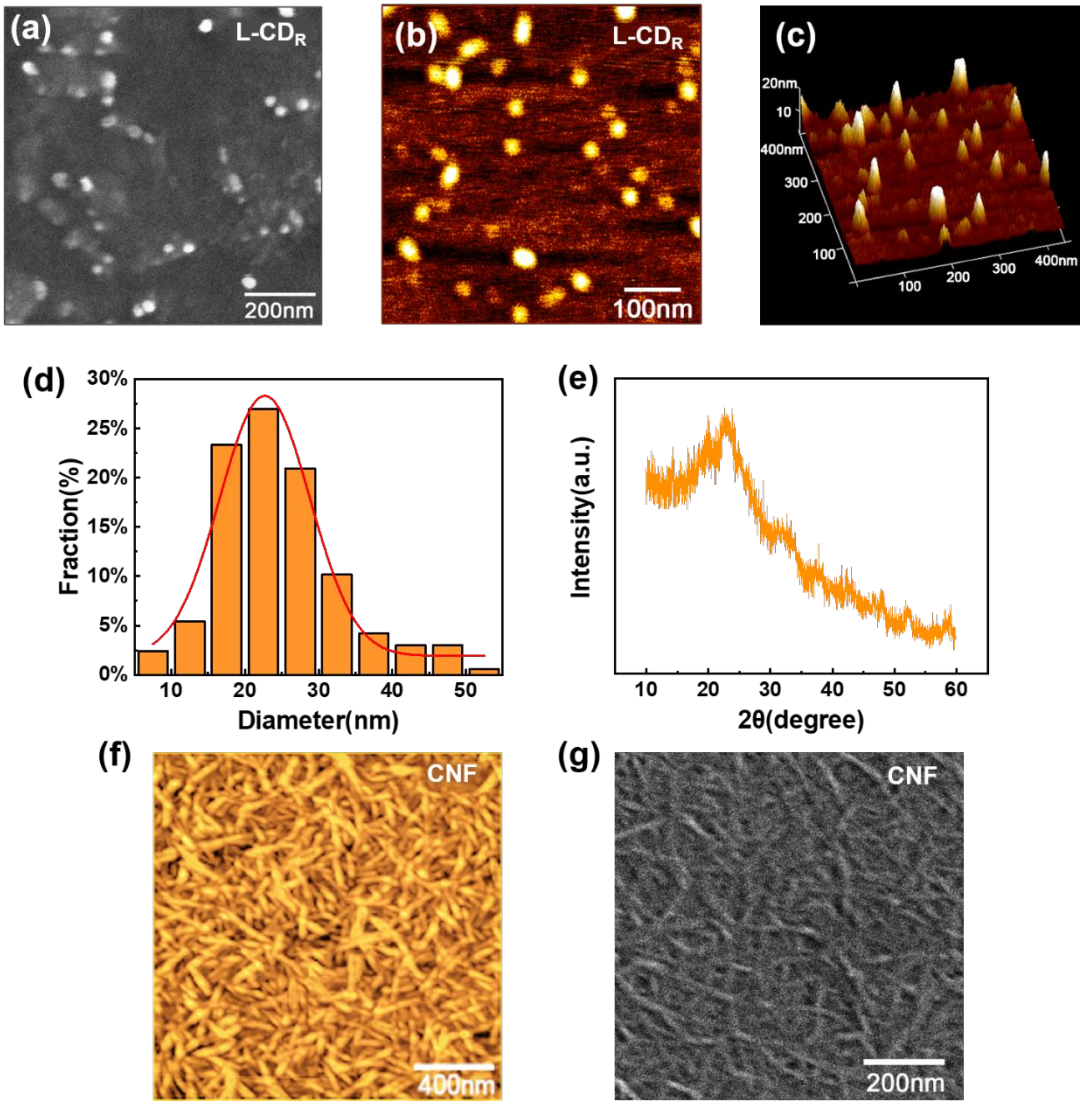

Figure 2. Characterization of L-CD and CNF. (**a**) SEM image of L-CD. (**b**) Surface and (**c**) 3D AFM images of L-CD. (**d**) Particle size distribution of L-CD, showing fabricated L-CD has a diameter of around 20 to 30 nm. (**e**) XRD pattern of L-CD. (**f**) AFM and (**g**) SEM images of CNF, demonstrating that CNF has a nanoscale size. The nanosized L-CD and CNF are beneficial to obtain high optical transparency hybrid films without loss of incident solar light for PSC devices.

View Article Online
DOI: 10.1039/D5TC02544C

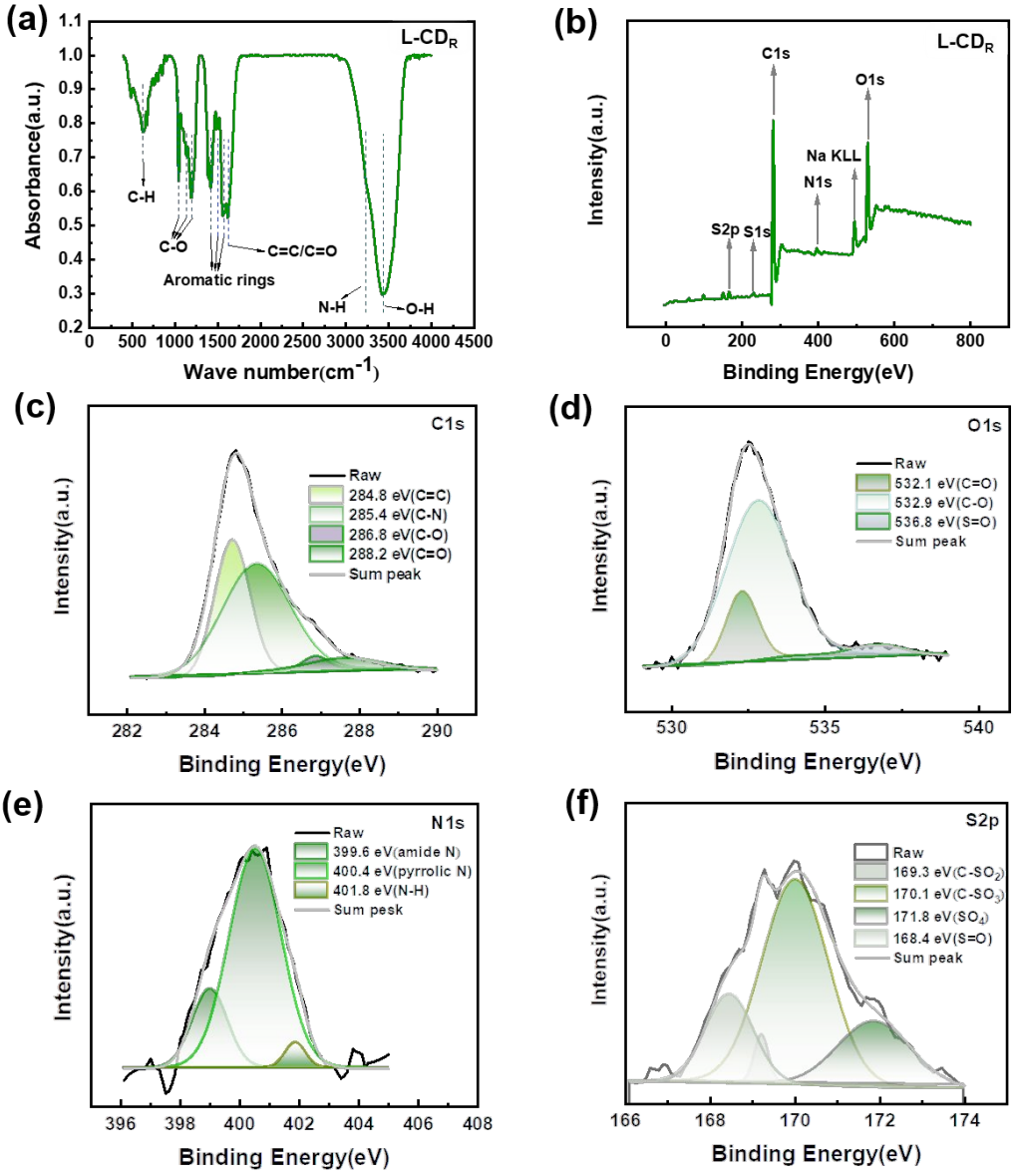

Figure 3. Infrared spectra and XPS spectra of L-CD_R. (**a**) Infrared spectra of the L-CD_R. (**b**) XPS spectra of L-CD. (**c**) C1s, (**d**) O1s, (**e**) N1s, and (**f**) S2p XPS spectra of L-CD_R. The results show the prepared L-CD_R has surface functional groups of -OH, C=O, and NH, etc.

View Article Online
DOI: 10.1039/D5TC02544C

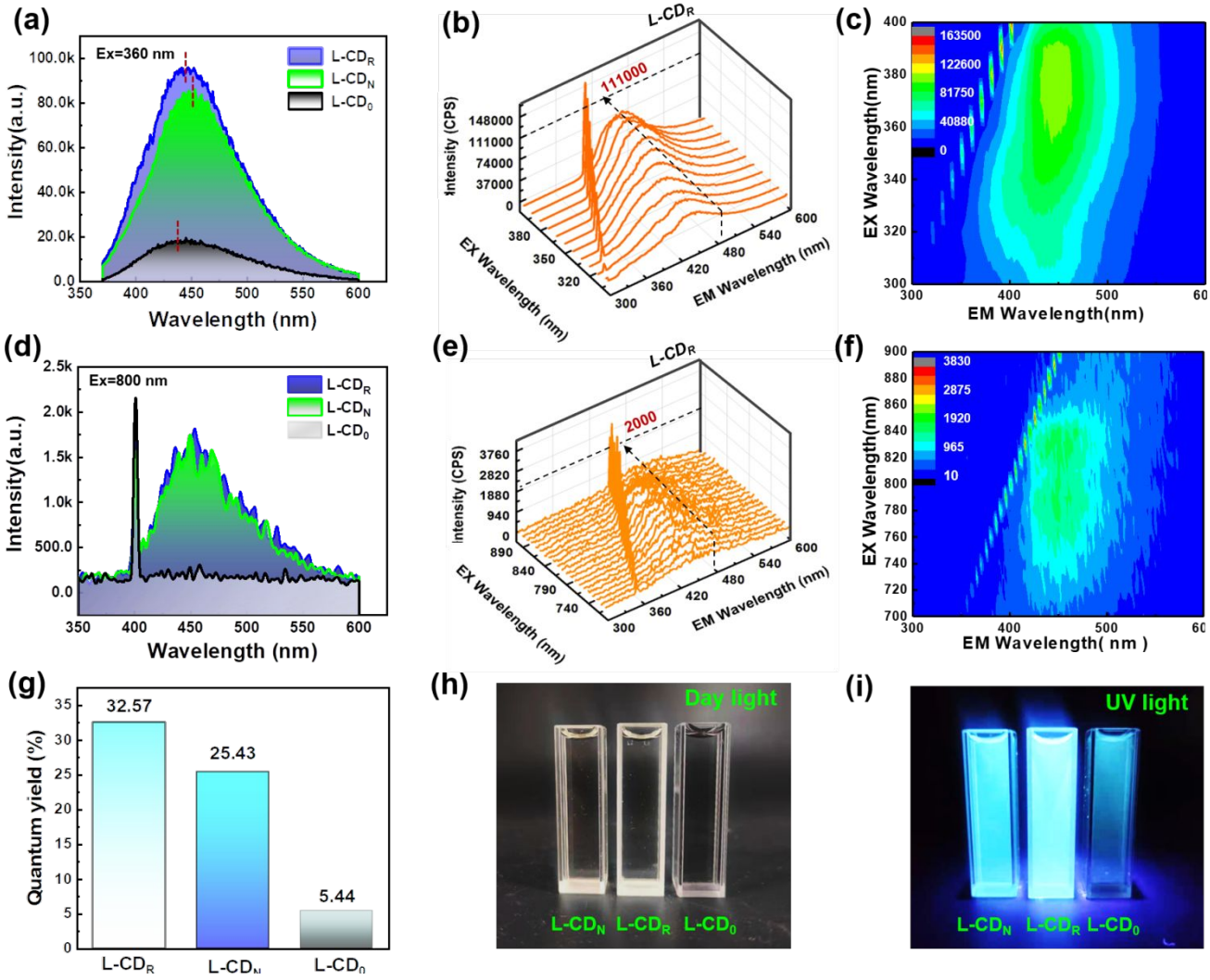

Figure 4. UV absorption, conversion, and fluorescence performance of lignin carbon dots. (**a**) Emission spectra of L-CD_0, L-CD_N, and L-CD_R with the excitation wavelength of 360 nm (λ_{ex}=360 nm), implying the reduced L-CD of L-CD_R has the best emission intensity. (**b**) 3D photoluminescence spectra and (**c**) the top view image of L-CD_R excited with the light in UV band, showing L-CD_R has excellent energy down-conversion properties and can convert UV light into visible light. (**d**) Emission spectra of L-CD_0, L-CD_N, and L-CD_R under the excitation wavelength of 800 nm (λ_{ex}=800 nm), demonstrating L-CD_N and L-CD_R have similar emission intensity over L-CD_0. (**e**) 3D photoluminescence spectra and (**f**) the top view image of L-CD_R excited with the

View Article Online
DOI: 10.1039/D5TC02544C

light in the NIR band, showing the L-CD_R has tiny up-conversion properties and can convert NIR into visible light. (**g**) Quantum yield of L-CD_0, L-CD_N, and L-CD_R. Digital photo images of lignin carbon dots under daylight (**h**) and UV light (**i**). The results show L-CD_R has strong energy down-conversion properties and weak energy up-conversion properties.

View Article Online
DOI: 10.1039/D5TC02544C

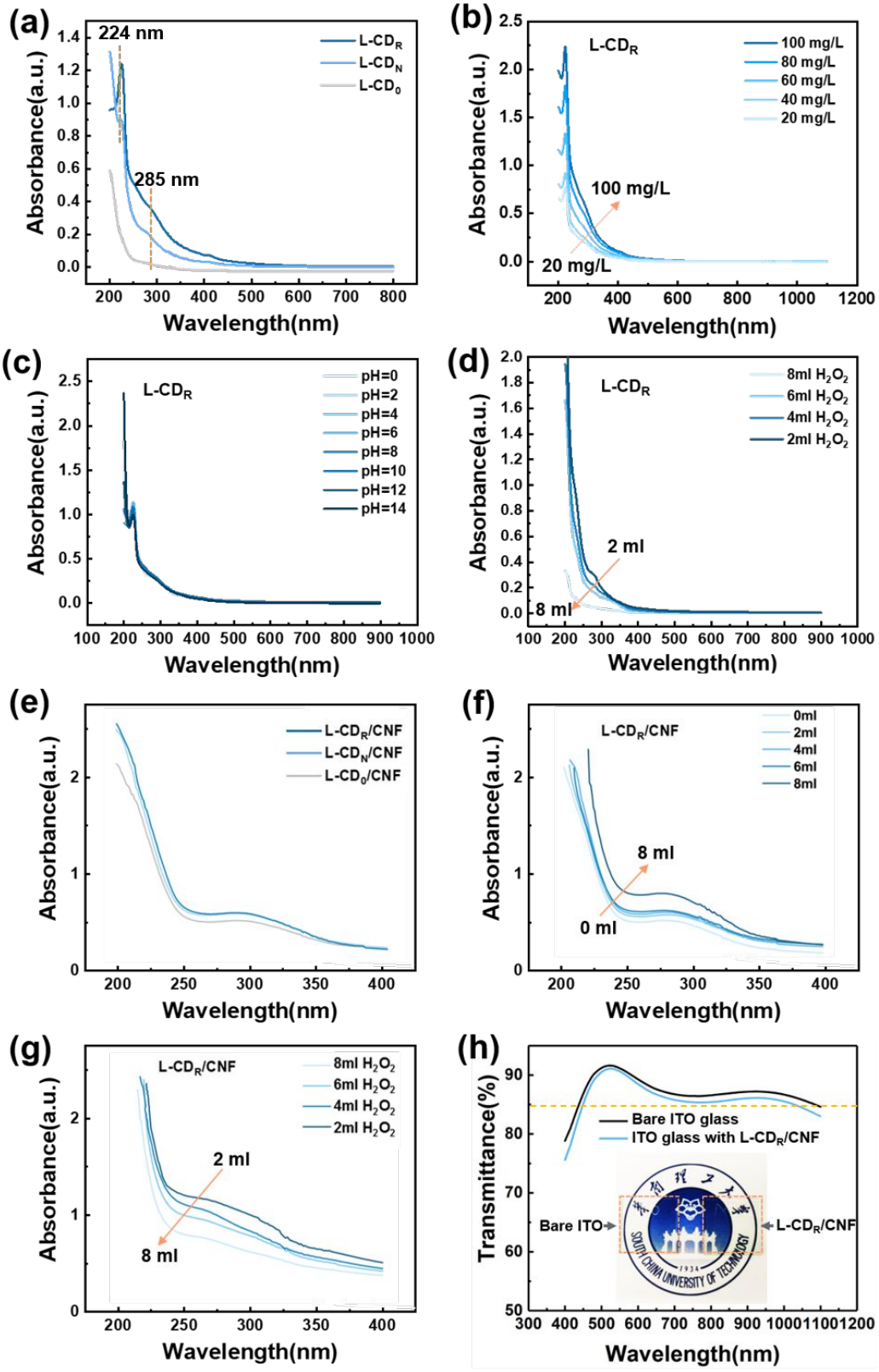

View Article Online
DOI: 10.1039/D5TC02544C

Figure 5. UV absorption optimization of different L-CD water solutions for L-CD/CNF film fabrication. (**a**) UV absorption spectra of L-CD_R, L-CD_N, and L-CD_0 solution. (**b**) UV absorption spectra of L-CD_R solution with different concentrations. (**c**) UV absorption spectra of L-CD_R with different pH values. (**d**) UV absorption spectra of L-CD_R produced with different amounts of H_2O_2. (**e**) UV absorption spectra of L-CD_R /CNF, L-CD_N /CNF, and L-CD_0 /CNF films. (**f**) UV absorption spectra of L-CD_R/CNF films with different volumes of L-CD_R addition. (**g**) UV absorption spectra of L-CD_R/CNF films with the L-CD_R treated with different amounts of H_2O_2. (**h**) Transmittance of ITO glass with and without L-CD_R/CNF films.

View Article Online
DOI: 10.1039/D5TC02544C

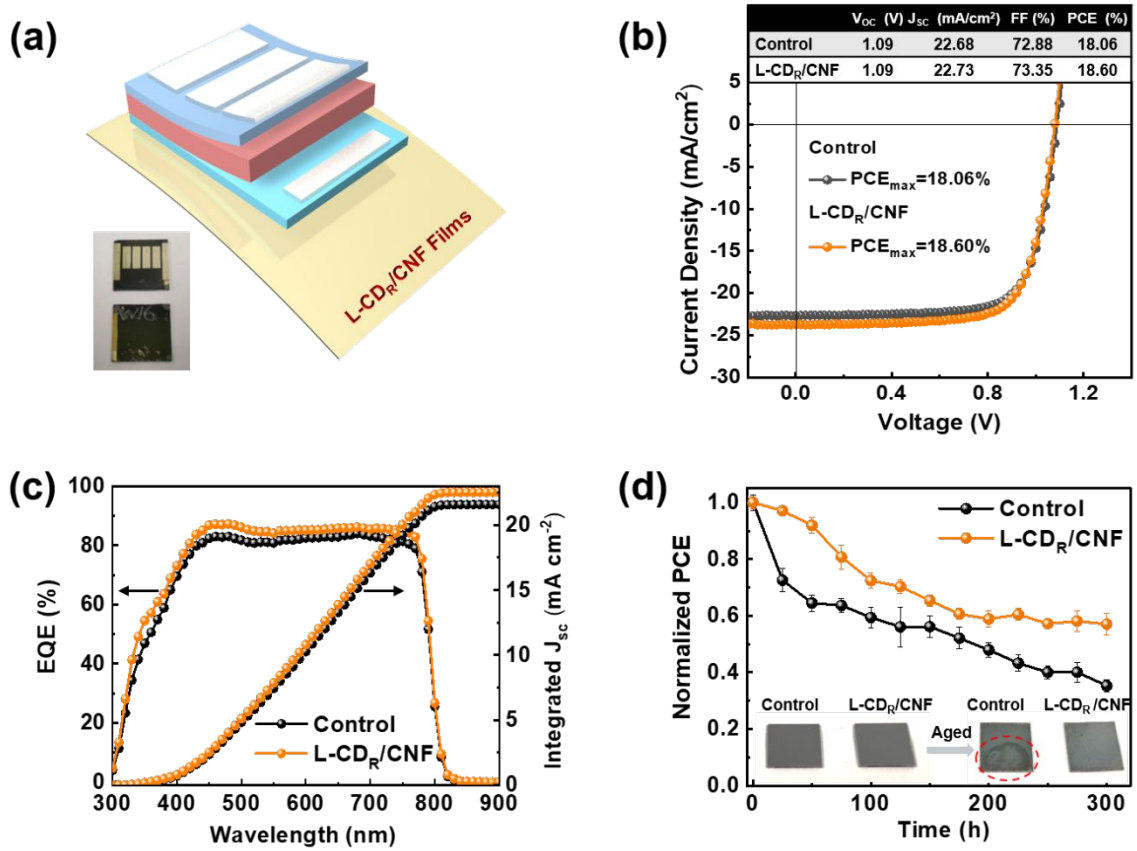

Figure 6. Effects of the L-CD_R/CNF films on PSC device performance. (**a**) Device structure based on L-CD_R/CNF films. (**b**) J-V curves of PSCs with and without L-CD_R/CNF films. (**c**) EQE spectra of the devices with and without L-CD_R/CNF films. (**d**) Stability of the PSC devices with and without L-CD/CNF films. The device performance is all improved which is attributed to the contribution of L-CD_R/CNF films.

View Article Online
DOI: 10.1039/D5TC02544C

Data availability statement

The authors confirm that the data supporting the findings of this study are available within the article and its supplementary materials.